Digital pulse processing ionization chamber pulses

Sh. Zeynalov[a], O. Zeynalova[ab], M. Nazarenko[b], F.-J. Hambsch[c], S. Oberstedt[c]

[a]*JINR-Joint Institute for Nuclear Research, Dubna, Moscow region, Russia*
[b]*Moscow State Institute of Radioengineering and Automation, 78 Vernadski Avenue, 119454 Moscow, Russia*
[c]*EC-JRC Institute for Reference Materials and Measurements, Retieseweg 111, 2440 Geel, Belgium*

Abstract. The purpose of the present paper was to report the recent results, obtained in development of digital pulse processing mathematics for prompt fission neutron (PFN) investigation using twin ionization chamber (TIC) along with fast neutron time-of-flight detector (ND). Due to well known ambiguities in literature (see refs. [4, 6, 9 and 11]), concerning a pulse induction on TIC electrodes by FF ionization, we first presented detailed mathematical analysis of fission fragment (FF) signal formation on TIC anode. The analysis was done using Ramo-Shockley theorem, which gives relation between charged particle motion between TIC electrodes and so called weighting potential. Weighting potential was calculated by direct numerical solution of Laplace equation (neglecting space charge) for the TIC geometry and ionization, caused by FF. Formulae for grid inefficiency (GI) correction and digital pulse processing algorithms for PFN time-of-flight measurements and pulse shape analysis are presented and discussed.

Keywords: Grid Inefficiency, ^{252}Cf(sf), Ionization chambers, Fission.
PACS: 29.30.Hs, 29.40.Cs, 29.40.Mc, 29.85.Fj, 25.85.Ca

INTRODUCTION

Nuclear fission model and prompt fission neutron emission (PFN) was first considered in classic paper of N. Bohr and J. Wheeler [1], where nuclei considered as a drop of charged liquid, which surface constantly distorted in competition between attractive nuclear and repulsive Coulomb forces. Rarely large distortion brought the nuclear into the configuration, where repulsion could not be compensated by nuclear force and the system split, sometimes after neutron emission. In this case the neutrons, called scission neutrons in order to distinguish them from the PFN, which are emitted from the fully accelerated fission fragments. First investigation of PFN emission was done in experiments [2, 3] in 1960-ies concluded that about 5 to 15% of fission neutrons were emitted before the fissile system split. Development of experimental technique and birth of commercial nuclear electronics allowed measurement of fission fragment (FF) and fission neutron kinematic parameters in a single fission event. In new experimental approach developed in ref. [4] authors investigated PFN emission in spontaneous fission of ^{252}Cf using twin Frish-grid ionization chamber (TIC) for FF kinetic energies and PFN emission angle along with PFN velocity measurement with help of liquid scintillator (NE213) based neutron detector (ND). Despite the authors demonstrated a power and high capacity of the new approach, some of their results (for example, dependence of average PFN multiplicity on total kinetic energy of FF) contained obvious contradictions with simple energy balance in fission. In present work we described further development of the experiment using modern digital pulse processing (DPP), implemented

with the detector signals along with in depth analysis of a signal induction on TIC electrodes by FF.

SIGNAL FORMATION ON TWIN IONIZATION CHAMBER ANODE

A sketch of the experimental setup with digital pulse processing electronics is shown in Fig. 1. A TIC was used for fission fragment mass-TKE and PFN emission angle (Θ) measurement. A target with fissile material, deposited on thin organic foil located on the common cathode of the chamber. Fission fragments were decelerated inside sensitive volume of two independent chambers spending their kinetic energy for free electron creation. Free electrons drifted inside the chamber to respective anodes. The electric charge, induced on two anodes and common cathode were proportional to fission fragments kinetic energy, are measured by three synchronized waveform digitizers (WFD). Approximately 0.15% of fission fragment detection coincided with neutron detection by ND, which signal was digitized using fourth WFD. The common time base was achieved due to all four digitizer was

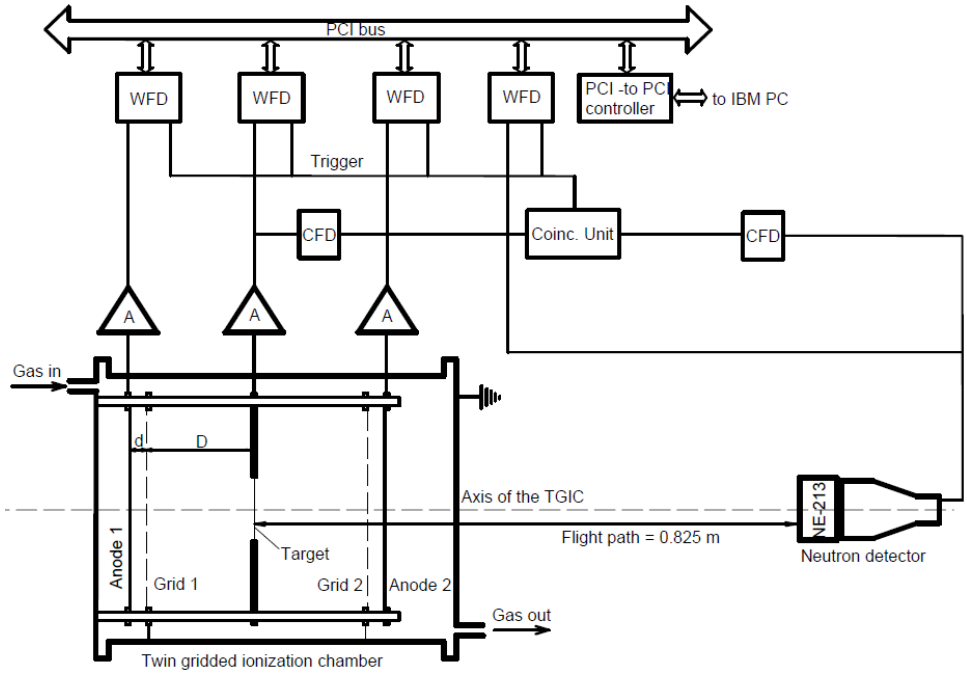

FIGURE 1. Scketch of experimental setup

sampling detector pulses synchronously and the common cathode pulse was considered as an indication of a fission event. The common cathode pulse was used as a "T-zero" signal for PFN time-of-flight measurement and as one of the input pulses of coincidence unit. A neutron, detected inside the time interval of 200 ns duration after "T-zero" was considered as PFN. In such a way two types of fission events were recorded in given experiment: with and without coincidence with ND pulse. Apparently, the intensity of fission events with coincidence with ND was proportional to conditional probability of neutron emission in a detected fission event. In given experiment the following parameters of fission event were required to be measured: kinetic energies of correlated FF, their angle in respect to the TIC axis, PFN time-of-flight and the angle between FF and PFN (thanks to allocation of ND on the TIC axis). The information about listed parameters was retrieved from the sampled TIC and ND pulses using DPP algorithms. The waveform of the anode signal, being preprocessed

by charge-sensitive preamplifier, was step-like pulse with height proportional to total charge of the electrons released during FF deceleration. The FF angle information can be obtained from the anode pulse rise time, which is proportional to the electron drift time from the point of origin to the respective anode. Relation between chamber geometry and the charge induction on the anode of TIC is given by the Ramo-Shockley theorem [5, 6]. According to the theorem a full charge, induced on the electrode by a moving charge can be calculated using a weighting electric field potential, calculated for all electrodes grounded except the considered one, which potential is raised to 1 V. In present work the calculation was done for a single cell with periodical boundary conditions in respect to x-axis of two dimensional Cartesian coordinates chosen as schematically shown in Fig. 2, where *D* and *d* are cathode-grid and grid-anode distances respectively. Dirichlet boundary conditions for this case required us to specify the potential along the boundaries: anode potential set to 1, cathode and grids both grounded, potential along the dotted lines set to linear rising function of y coordinate from the zero at the cathode to 1 at the anode.

The electric potential can be found as the solution of Laplace equation

$$\frac{\partial^2 F(x,y)}{\partial x^2} + \frac{\partial^2 F(x,y)}{\partial y^2} = 0 \tag{1}$$

satisfying to described above boundary conditions. To solve eq. 1 numerically the inside of the rectangular cell was covered with a uniform computational grid with pitch h and the following finite difference approximation formulae were used:

$$\frac{\partial^2 F}{\partial x^2} = \frac{2F_v}{v(v+q)} + \frac{2F_q}{q(q+v)} - \frac{2F_o}{qv}, \qquad \frac{\partial^2 F}{\partial y^2} = \frac{2F_p}{p(p+u)} + \frac{2F_u}{u(p+u)} - \frac{2F_o}{pu}$$

$$\frac{F_v}{v(v+q)} + \frac{F_q}{q(v+q)} + \frac{F_p}{p(p+u)} + \frac{F_u}{u(p+u)} = \frac{pu+qv}{puqv} F_o \text{ - finite difference Laplace equation} \tag{2}$$

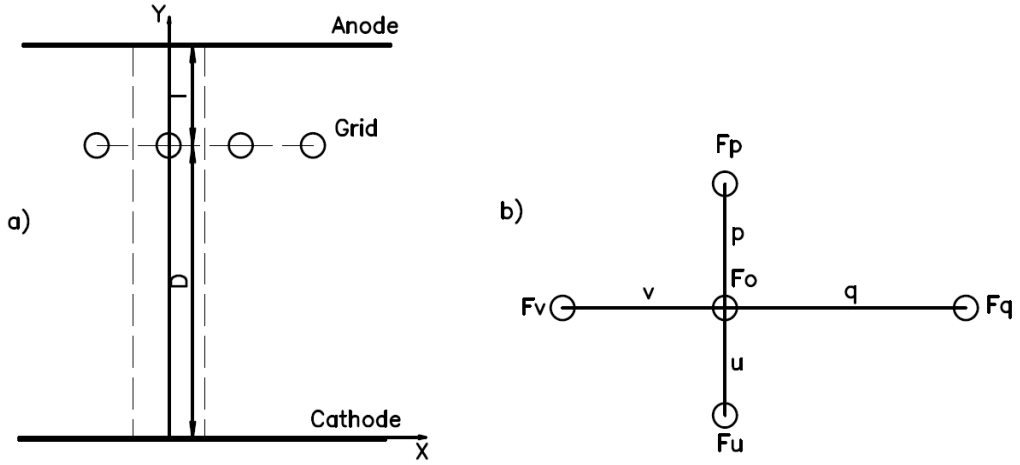

FIGURE 2 a) Area, confined by dashed lines, where the Laplace equation solved with periodical Dirichlet boundary conditions. b) generalized finite difference scheme demonstrating how the second order derivatives were calculated at the grid node F_0 using adjacent nodes F_q , F_p , F_p *and* F_v

When the point F_o was far enough from the grid the distances *p,q,u* and *v* were supposed to be equal to the chosen pitch *h*. When at least one point crossed the grid boundary, then the

corresponding distance was set to the distance between F_o and the boundary. The obtained solution F(x,y) was integrated over x-coordinate and plotted in Fig. 3a as $F_x(y)$.

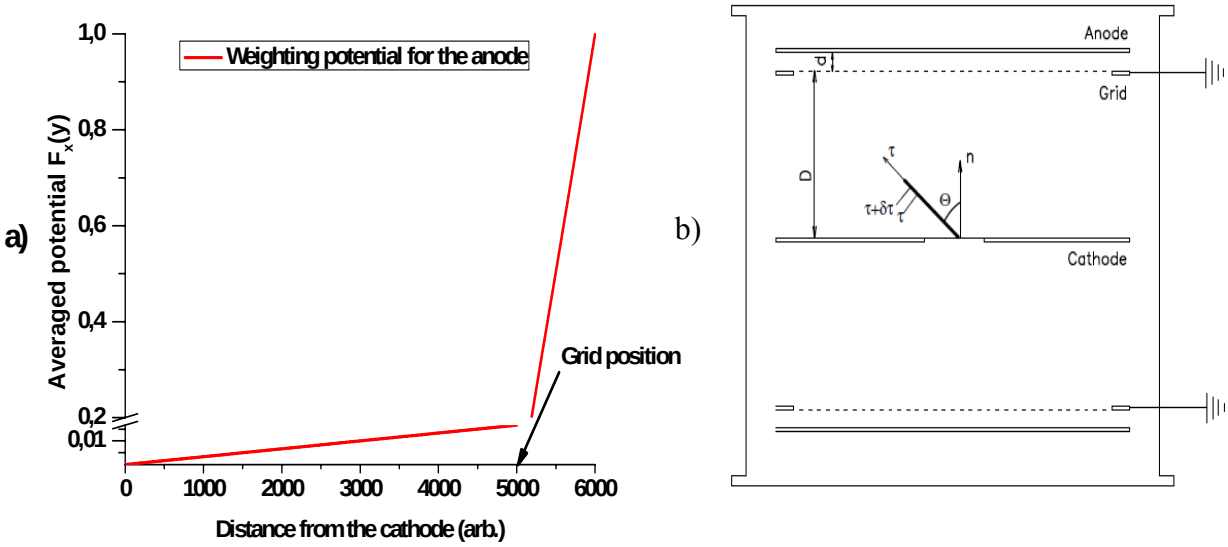

FIGURE 3. a) Weighting potential for the anode b) Illustration of the free electron drift in TIC.

Charge induced on the anode when free electrons with total charge q are drifting from the point of origin τ (we suppose that the τ-axis aligned along the FF motion direction) to a point with potential $F_x(y)$ can be calculated using the following formula:

$$Q(y) = (F_x(y) - F_x(y = \tau \times \cos(\Theta)) \times q \qquad (3),$$

where subscript x in $\boldsymbol{F_x(y)}$ denotes averaging of calculated weighting potential $\boldsymbol{F(x,y)}$ in respect to $\boldsymbol{x}$. The following dependence of averaged weighting on $\boldsymbol{y}$ was obtained and plotted in Fig. 3a:

$$F_x(y) = \begin{cases} \sigma \dfrac{y}{D} \text{ for } 0 \le y < D \\ (1-\sigma)\dfrac{y-D}{l} + \sigma \text{ for } \mathrm{D} \le \mathrm{y} \le \mathrm{D}+1 \end{cases} \qquad (4)$$

The parameter $\boldsymbol{\sigma}$ – is a grid inefficiency factor [6] and eq. 3 gives charge $\boldsymbol{q=\rho(\tau)d\tau}$, induced by the electrons in the interval $\boldsymbol{(\tau,\ \tau+d\tau)}$ when they drifted from the point of origin to the point, having potential $\boldsymbol{F_x(y)}$, the induced charge $\boldsymbol{dQ(y)}$ can be expressed as

$$dQ(y) = ((1-\sigma) \times \frac{y-D}{l} + \sigma - \sigma \times \frac{\tau \times \cos(\Theta)}{D})\rho(\tau)d\tau \qquad (5)$$

Assuming all FF decelerated inside the cathode-grid area and integrating eq. 5 over $\boldsymbol{\tau}$ gives the charge Q, induced by whole electrons along a FF deceleration path, when they collected on the anode as:

$$Q(D+d)=\int_0^L e\times\rho(\tau)\times(1-\sigma\times\frac{\tau\times\cos(\Theta)}{D})d\tau=N\times e\times(1-\sigma\frac{\hat{X}\times\cos(\Theta)}{D}) \quad (6)$$

In eq. 6 the $\hat{X}=\int_0^L \tau\times\rho(\tau)d\tau$ is the "centre of charge" and $N=\int_0^L \rho(x)dx$ is a total number of electrons, created during the FF deceleration. Drift time ***T*** of the "charge centre" of FF ionization from the point of origin to the point with coordinate $y=D+\frac{l}{2}$ can be calculated as:

$$T=\frac{D}{W}(1+\frac{l}{2D}-\frac{\bar{X}}{D}\cos(\Theta)) \quad (7)$$

Eq. 7 describes dependence of drift time *T* on *cos(Θ)*. The DPP algorithms and practical implementation of pulse height and angle evaluation were described in previous papers [7-9]. In next chapter we are providing some new results related to PFN time-of-flight spectroscopy.

DPP FOR PROMPT FISSION NEUTRON TIME-OF-FLIGHT SPECTROSCOPY

Measurement of PFN time-of-flight in present experiment we used cathode pulse of TIC as a "T-zero" signal and the ND signal as "Stop" signal. Time difference between these two signals was considered as the PFN time-of-flight (TOF). Narrow bandwidth (100 MHz sampling) available in our measurements and wide pulse height range (~100) of ND pulses, made data analysis more complicated due to some surprising effects was not foreseen beforehand. ND, used in experiment, was sensitive to prompt fission gamma radiation and this fact became helpful to overcome the limitation of narrow bandwidth of the apparatus.
The bandwidth of ND pulse can be evaluated from the pulse rise time, which was found to be ~100 MHz for ~4 ns rise time. Because of 100 MHz sampling frequency and taking into account Shannon sampling theorem the signal bandwidth was limited with help of anti-aliasing filter of 4-th order (Bessel filter with 45 MHz cutoff frequency). Before data analysis ND waveform passed additional 4-th order digital Butterworth filter, constructed using algorithm described in ref. [7]. Constant fraction time triggering (CFTT) was implemented digitally to measure the time difference between TIC cathode and ND pulse. It is well known that CFTT works well when it is implemented to pulses, having identical rise times. In present measurement scheme the identity of ND pulses was guaranteed by filters, applied to ND signals as was described above. Constant fraction value was selected 0.2 of pulse height and parabolic interpolation was implemented between successive samples. Resulting TOF distribution measured using considered approach and pulse shape separation of neutrons from gamma radiation presented in Fig.4a. In order to demonstrate the effects, distorting the shape of the TOF plot from Fig. 4a, two-dimensional plot in coordinates TOF – ND total light output was plotted in Fig. 4b. The points on the Fig. 4b, corresponding to gamma-radiation, demonstrate obvious dependence on the total light output (proportional to ND pulse height). We explained that dependence by the filters, introduced additional phase delay for ND pulses. To correct those phase delays we first parameterized gamma radiation shift on the ND pulse height using linear approximation. Then the shift corrected for both neutron and gamma radiation pulses in similar way during data analysis. Result after correction presented on Fig. 5 and looks more reasonable in comparison with Maxwell distribution with parameters taken

from ref. [4]. It should be noticed that problems related to phase delays are quite complicated for investigation using pure theoretical approach and should be combined with experimental methods.

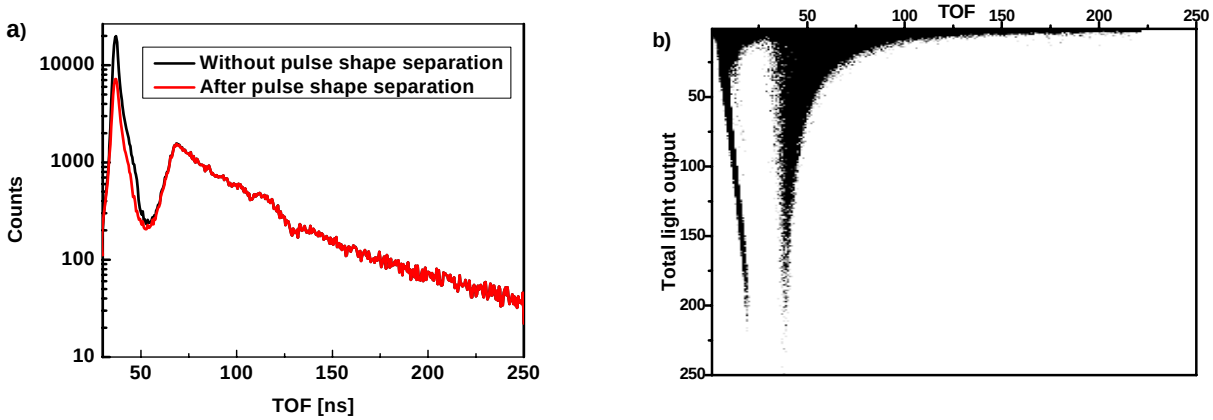

FIGURE 4. a) TOF distribution obtained using digital CFTT method. b) Two-dimensional plot in coordinates TOF-ND total light output.

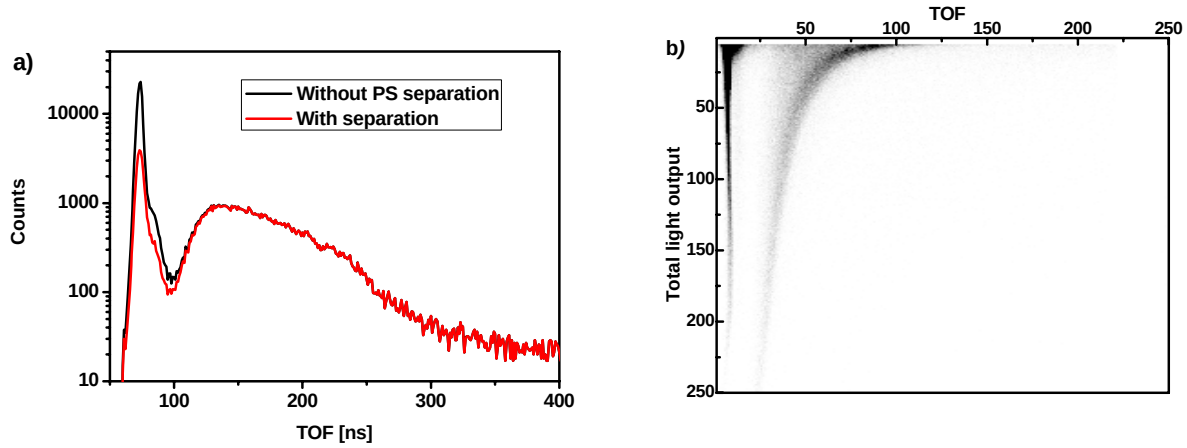

FIGURE 5. Application of mathematical analysis of signal formation in TIC and developed DPP algorithms for prompt fission neutron TOF spectroscopy allowed us to avoid some uncertainties and correct the final results of PFN emission. a) time-of-flight distribution after correction for pulse height dependence and pulse shape analysis, b) Two-dimensional TOF-ND plot after correction.

DISCUSSION

Our result concerning grid inefficiency (GI) correction factor, deducted from eq. 6, is in very good agreement with paper from ref. [6] and early result published in ref. [10]. It should be noticed that in recent years there was another point of view to GI factor correction published in ref. [11], where experimental method of GI factor determination with help of digitized anode signal waveform was provided. Eq. 6 in present work was deducted from classic electrodynamics (see ref. [5]) and reflects the electrostatic induction of charges, moving in the electrostatic field, created by the electrodes of TIC (Fig. 3a). Both authors of ref. [10] and ref. [11] used correction of eq. 6 in order to eliminate effect of angular dependence. In case of ref. [10] the goal was achieved by addition to eq. 6 of the

term $Ne\sigma\frac{\hat{X}\cos(\Theta)}{D}$, and subtraction of the term $Ne\sigma(1-\frac{\hat{X}\cos(\Theta)}{D})$ in case of ref. [11]. From practical point of view both approaches bring to correct results, when proper spectrometer energy calibration procedure was implemented. For example, when one calibrates the energy scale of spectrometer with alpha particles with extrapolation to FF energy range then approach of ref. [10] would be more precise, because it does not introduce additional shift of $Ne\sigma$. In case of the energy scale calibration using known average heavy and light FF kinetic energy values both approaches will bring to the same results because any systematic shift is eliminated in the energy calibrating.

ACKNOWLEDGMENTS

This work partially was supported by RFBR grant 10-07-00541a.

REFERENCES

1. N. Bohr, J.A. Wheeler, *Physical Review*, 56, pp. 426-450 (1939)
2. H. R. Bowman, S. G. Thompson, J. C. D. Milton, W. J. Swiatecki, *Physical Review,* 126, pp. 2120-2136, (1962)
3. K. Skarsvag, K. Bergheim, *Nucl. Phys.,* 45, pp. 72-97, (1963).
4. C. Budtz-Jørgensen and H.-H. Knitter , *Nucl. Phys.*, **A490**, 307- 328 (1988).
5. W. Shockley, *Journal of Applied Physics,* 9, pp. 635-636 (1938).
6. A. Göök, F.-J. Hambsch, A. Oberstedt and S. Oberstedt, submitted to Nucl. Instr. Meth. A.
7. O. Zeynalova, Sh. Zeynalov , F.-J. Hambsch and S. Oberstedt, "DSP Algorithms for Fission Fragment and Prompt Fission Neutron Spectroscopy in *Application of Mathematics in Technical and Natural Sciences-2010,* edited by M. D. Todorov and C. I. Christov, AIP Conference Proceedings 1301, American Institute of Physics, Melville, NY, 2010, pp. 430-439.
8. O.V. Zeynalova, Sh.S. Zeynalov, F.-J. Hambsch, S. Oberstedt, *Bulletin of Russian Academy of Science: Physics*, 73, pp. 506-514 (2009).
9. A. Al-Adili, F.-J. Hambsch, S. Oberstedt, S. Pomp, Sh. Zeynalov, *Nucl. Instr. Meth.* **A624***,* pp. 684-690 (2010).
10. C. Budtz-Jorgensen, H. H. Knitter, Ch Straede, F. J. Hambsch, R. Vogt, *Nuclear Instruments and Methods in Physics Research Section A,* 258, pp. 209- 220 (1987).
11. V.A. Khriachkov, et al., *Nuclear Instruments and Methods in Physics Research Section A*, 394, pp. 261-265, (1997).